How to cite: *Angew. Chem. Int. Ed.* **2021**, *60*, 23365 – 23372
International Edition: doi.org/10.1002/anie.202110043
German Edition: doi.org/10.1002/ange.202110043

Photochemistry

Bright Luminescence in Three Phases—A Combined Synthetic, Spectroscopic and Theoretical Approach

Milena Dahlen, Eike H. Hollesen, Max Kehry, Michael T. Gamer, Sergei Lebedkin, Detlef Schooss, Manfred M. Kappes, Wim Klopper,* and Peter W. Roesky**

Abstract: *Combining phase-dependent photoluminescence (PL) measurements and quantum chemical calculations is a powerful approach to help understand the influence of the molecular surroundings on the PL properties. Herein, a phosphine functionalized amidinate was used to synthesize a recently presented bimetallic gold complex, featuring an unusual charge separation. The latter was subsequently used as metalloligand to yield heterotetrametallic complexes with an Au-M-M-Au "molecular wire" arrangement (M = Cu, Ag, Au) featuring metallophilic interactions. All compounds show bright phosphorescence in the solid state, also at ambient temperature. The effect of the molecular environment on the PL was studied in detail for these tetrametallic complexes by comparative measurements in solution, in the solid state and in the gas phase and contrasted to time-dependent density functional theory computations.*

Introduction

Systematic photophysical investigations regarding a defined ligand system with varying metal loadings in the context of luminescence properties are rather scarce.[1] It is well known that in condensed phase, packing effects or interactions with counterions and solvent molecules can have a significant impact on the photophysical properties.[2] Investigating these properties by quantum chemical calculations thus introduces an additional layer of complexity due to the various intermolecular effects present in dynamic systems, like in solutions or in a solid. These factors contribute to challenges in establishing structure–property correlations for various classes of metal–organic compounds.[3] In this work, we combined conventional condensed phase studies of a series of photoluminescent tetranuclear homo- and heterometallic coinage metal complexes with gas phase PL measurements and quantum chemical calculations. The aim was not only to provide a more reliable comparison between experiment and theory, but also to gain insights into the effects of molecular surroundings on the photophysical properties.

Specifically, from a synthetic point of view, we present herein a series of coinage metal complexes of *N,N′*-bis[(2-diphenylphosphino)phenyl]formamidinate (dpfam), an established monoanionic P^N^N^P ligand (Scheme 1), featuring both "soft" and "hard" coordination sites according to the

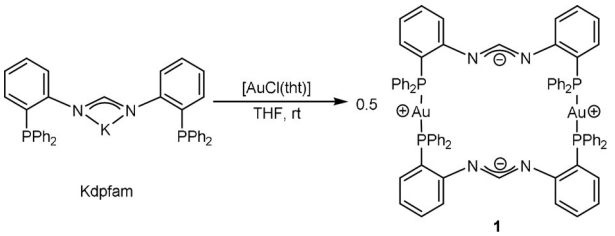

Scheme 1. Synthetic pathway towards the binuclear gold complex $[dpfam_2Au_2]$ (**1**).[12]

"hard and soft acids and bases" (HSAB) principle.[4] The different sites have been used following a building block strategy as illustrated in Figure 1. According to this, the outer "soft" phosphine donors are first bound to gold cations. In the second step, the vacant amidinate pocket is selectively filled with metal cations, resulting in tetranuclear complexes. Importantly, all these complexes feature pronounced metal-

[*] M. Dahlen, Dr. M. T. Gamer, Prof. Dr. P. W. Roesky
Institute of Inorganic Chemistry
Karlsruhe Institute of Technology (KIT)
Engesserstrasse 15, 76131 Karlsruhe (Germany)
E-mail: roesky@kit.edu
E. H. Hollesen, Dr. S. Lebedkin, Priv. Doz. Dr. D. Schooss, Prof. Dr. M. M. Kappes
Institute of Nanotechnology
Karlsruhe Institute of Technology (KIT)
Hermann-von-Helmholtz-Platz 1, 76344 Eggenstein-Leopoldshafen (Germany)
E-mail: manfred.kappes@kit.edu
M. Kehry, Prof. Dr. W. Klopper
Karlsruhe Institute of Technology (KIT)
Institute of Physical Chemistry (Theoretical Chemistry)
Kaiserstrasse 12, 76131 Karlsruhe (Germany)
E-mail: klopper@kit.edu
Prof. Dr. M. M. Kappes
Institute of Physical Chemistry
Karlsruhe Institute of Technology (KIT)
Fritz-Haber-Weg 2, 76131 Karlsruhe (Germany)

Supporting information (experimental details) and the ORCID identification number(s) for the author(s) of this article can be found under:
https://doi.org/10.1002/anie.202110043.

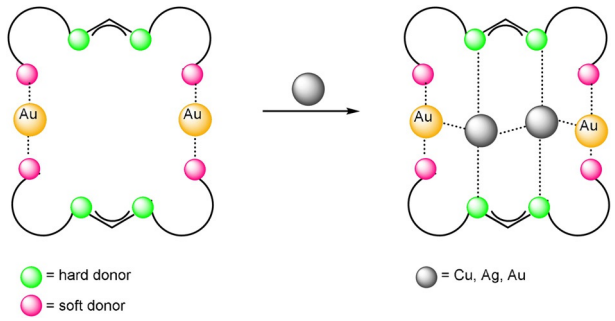

Figure 1. "Building block" strategy towards tetrametallic complexes using different hard and soft coordination sites.

lophilic interactions which are facilitated via the supporting dpfam ligand system.[5]

Metallophilic interactions have been the subject of experimental and theoretical research during the last decades.[6] In general, metallophilicity describes the tendency of metallo-organic compounds to manifest closer metal center separations than expected for charge centers with equal polarity, often being shorter than the van der Waals distance. First mostly correlated with gold,[7] the discovery of similar behavior for other late d-block and heavy p-block elements in low oxidation states showed that this "metallophilicity" phenomenon is, in fact, not unusual.[5,8] However, their origin is still subject of discussion.[6b,9]

Latter interactions are known for their potential influence on the often observed manifold photophysical properties for compounds comprising metallophilic contacts.[9b,10] For heavy metals such as gold, efficient intersystem crossing (ISC) is observed due to enhanced spin–orbit coupling, leading predominantly to phosphorescence with emission decay times typically in the microsecond range.[9b] Tuning these photoluminescence properties by structural modification is of applications interest in fields ranging from OLED design and sensor technology to tumor markers.[8c,11] Here we tune the metallophilic interactions in a range of Au-M-M-Au complexes by varying composition.

The PL properties of the tetranuclear complexes were studied in the solid state over a broad range of temperatures down to 20 K and—for $[dpfam_2Au_2M_2]^{2+}$ (M = Cu, Au)—in solution and gas phase. These measurements were complemented by DFT and TDDFT calculations of the electronic excitations. To the best of our knowledge, this is the first example of combined phase-dependent PL studies, including gas phase, and theoretical studies for metal–organic compounds.

Results and Discussion

To realize the above building block strategy, the phosphine moieties were first loaded with the "soft" gold(I) cation (see Figure 1). Ligand precursor Kdpfam[12] was therefore subjected to a salt metathesis reaction with tetrahydrothiophene gold chloride [AuCl(tht)], yielding the binuclear gold compound $[dpfam_2Au_2]$ (**1**, Scheme 1).[12] Each gold cation is herein coordinated by two phosphine moieties in an almost linear fashion (Scheme 1). Although the nitrogen atoms are negatively charged, the "soft" gold cations prefer the "soft" phosphine atoms, resulting in a remarkable charge separation.[12] This selective coordination leaves the expected free coordination sites on the nitrogen atoms, which can be exploited in the second step to obtain tetrametallic complexes.

Tetrametallic Complexes

Following the building block strategy, we next implemented metal cations (Cu^I, Ag^I and Au^I) into the vacant amidinate coordination pocket of metalloligand **1**. Homo and hetero tetrametallic complexes were synthesized by reaction of **1** with $[Cu(MeCN)_4][PF_6]$, $[AgBF_4]$, or $[Au(tht)_2][BF_4]$ resulting in $[dpfam_2Au_2Cu_2][PF_6]_2$ (**2**), $[dpfam_2Au_2Ag_2][BF_4]_2$ (**3**), and $[dpfam_2Au_4][BF_4]_2$ (**4**), respectively (Scheme 2). After stirring each reaction mixture in THF overnight, the formed precipitate was redissolved by adding small amounts of acetonitrile and subsequent heating. Storing the solutions overnight led to crystalline products (yields: 58% (**2**), 49% (**3**), and 19% (**4**)).

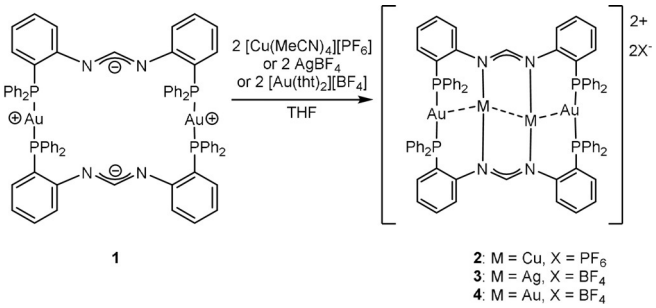

Scheme 2. Synthetic strategy towards the heterotetrametallic complexes **2**–**4**.

Compound **2** was obtained as yellow crystals which show bright yellow luminescence under UV light (see Figure 3). The solid-state structure of **2** (Figure 2) revealed an Au-Cu-Cu-Au zigzag chain with intermetallic angles of 119.75(10)° and 124.08(10)°. Intermetallic distances were determined to be 2.594(3) Å for Cu1–Cu2 and 2.832(2) Å (Au1–Cu1) and 2.806(2) Å (Au2–Cu2) for the heterometallic Au–Cu contacts, being within the range of strong metallophilic interactions.[13] The copper atoms are each coordinated by two nitrogen atoms of the amidinate units and by the oxygen of one half occupied and disordered THF molecule. Additional metallophilic contacts to gold and another copper atom complete the distorted trigonal bipyramidal coordination sphere (Figure 2). Ignoring the Au–Cu contacts, both gold atoms are each coordinated by two phosphine moieties in an almost linear fashion. The P-Au-P angle is bent from ideal 180° to 174.95(13)° (P5-Au1-P5′) and 169.2(2)° (P6-Au2-P6′).

Similarly, N-Cu-N angles are approximately identical (172.1(6)° and 171.5(6)°). Alike N–C bond lengths indicate a delocalization of the negative charge between the nitrogen atoms. The $^{31}P\{^1H\}$ NMR spectrum showed two resonances:

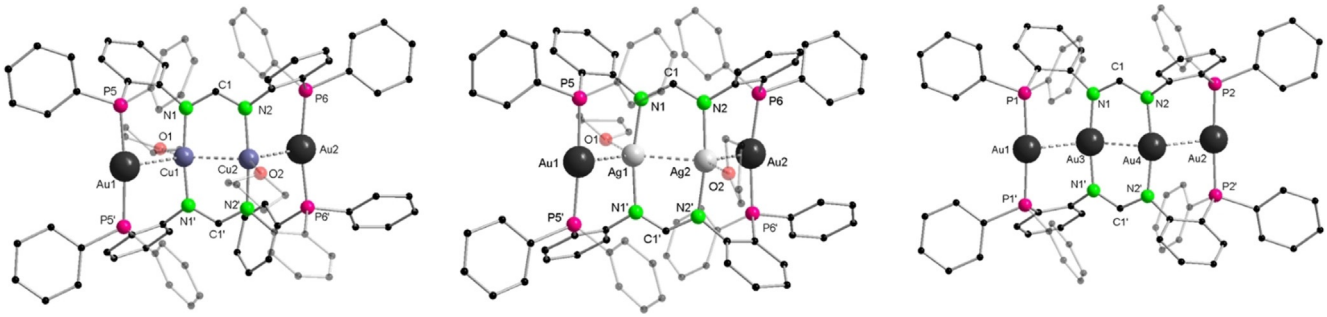

Figure 2. Molecular structures of the cations of the tetrametallic complexes **2** (left), **3** (middle), and **4** (right) in the solid state.[28] Hydrogen atoms and non-coordinating solvent molecules are omitted for clarity. The THF molecules shown are not fully occupied and disordered over two positions (see SI). Selected bond lengths and angles are given in the Supporting Information.

a broad singlet at $\delta = 33.8$ ppm for the ligands' phosphorous atoms and a characteristic septet at $\delta = -144.6$ ppm for the counterion $[PF_6]^-$. High-resolution mass spectrometry (HRMS) and elemental analysis further supported the structural data. In 2006, Lagunas et al. reported within a hexanuclear complex a comparable (partly ligand unsupported) Au-Cu-Cu-Au zigzag motif. They observed a much smaller angle of Au1-Cu1-Cu1′ (73.98(6)°) and a slightly longer Cu–Cu distance (2.898(3) Å) while the Au–Cu bond length is almost identical to that in **2**.[13b]

Colorless crystals of the corresponding isostructural silver compound **3** exhibit a blueish luminescence when excited with a UV lamp. In the solid state, the tetrametallic Au-Ag-Ag-Au chain shows angles of 121.93(7)° (Ag2-Ag1-Au1) and 116.91(7)° (Ag1-Ag2-Au2) and features intermetallic interactions with bond lengths of 2.900(2) Å (Au1–Ag1), Au2–Ag2 2.876(2) Å and 2.734(2) Å (Ag1–Ag2, Figure 2).[14] Phosphine-gold-phosphine angles differ from each other by approximately 6° (176.2(2)° and 170.3(2)°). The metal cations are settled in the same coordination environment as in **2** with the silver atoms being in a trigonal bipyramidal (coordination of partially occupied THF molecules) and the gold atoms, including the Au-Ag contacts, in an almost planar T-shaped coordination sphere (Figure 2). The $^{31}P\{^1H\}$ resonance of **3** was detected as a broad singlet at $\delta = 35.5$ ppm. HRMS further supported the elemental composition of **3**. A similar structural motif was reported by Hector and co-workers in 2010. However, their determined Ag–Ag (3.0129(14) Å) as well as Au–Ag distances (3.2113(9) Å) are significantly longer than observed in **3**.[14] Gimeno, Lopez-de-Luzuriaga et al. also reported in 2017 a tetranuclear metal chain featuring partially unsupported heterometallophilic (Ag–Au) interactions in a bent arrangement (Au-Ag-Ag 145.66(2)°).[15] The intermetallic distances in that complex correspond well to those in **3** despite the more rigid environment provided by the tetradentate dpfam ligand.

To complete the coinage metal series, the homometallic tetranuclear gold complex **4** was prepared. Accordingly, $[Au(tht)_2][BF_4]$ was first prepared in situ before being reacted with **1**. The colorless crystals of **4** manifest an intense greenish luminescence (see Figure 3). Single X-ray diffraction revealed compound **4** to be almost isostructural to **2** and **3** (Figure 2). However, there is no coordinating solvent on the gold atoms leading to almost linearly coordinated gold cations (P1-Au1-P1 175.9(2)°, P2-Au2-P2 175.9(2)°, N2-Au4-N2 169.3(6)°, N1-Au3-N1 171.8(5)°). Within the Au-Au-Au-Au zigzag chain, short intermetallic distances of 2.8850(9) Å, 2.8577(10) Å, and 2.6998(8) Å indicate aurophilic interactions and are in accordance with literature values.[5,8h,16] Compared to **2** and **3**, the intermetallic angle is significantly wider (132.38(3)° and 130.88(3)°) whilst the amidinate N-C-N angle increased only slightly (125.5(12)°). In CD_3CN, **4** showed a dynamic behavior, leading to non-interpretable NMR spectra. $^{31}P\{^1H\}$ NMR spectroscopy in DMSO-d_6 however revealed a singlet resonance at $\delta = 29.6$ ppm, which is in a comparable range as for **2** and **3**. ^1H NMR spectroscopy in DMSO-d_6 showed one set of signals as observed for **2** and **3**. Furthermore, **4** was identified unambiguously by HRMS and elemental analysis. A related Au_4-chain with supported metallophilic contacts was presented in 1993 by Mak et al. and in 2014 by Tanase et al.[17] In those previous Au_4-chains, gold cations are in a more linear arrangement and the reported intermetallic distances are slightly longer (ca. 2.9–3.1 Å) than those found for **4**.[17]

All three tetrametallic compounds **2**–**4** feature an Au-M-M-Au chain with metal–metal distances below the sum of their corresponding van der Waals radii and within typical values for metallophilic interactions.[13b,14–15] While in **2** and **3** the intermetallic angles are almost identical, they are widened significantly in **4** (see also Table S6-1 in the Supporting Information).

A comparison with literature reports leads to the conclusion that the dpfam ligand provides a suitable scaffold to enable and support shorter intermetallic distances than in other reported supporting ligand systems.[13b] However, the ligand steric demand is too high or its capacity too small to allow a linear arrangement as is found in unsupported systems or systems with less steric demand.[15,17a]

Photoluminescence Properties

Complexes **2**–**4** with chains of four metal atoms and pronounced metallophilic interactions all showed room temperature luminescence and were subject of photophysical investigations at various temperatures and in different physical states. Figure 3 shows PL spectra of **2**–**4** in solid state at different temperatures. The relatively broad (especially in case of **2**) emission maxima at 530 nm, 430 nm and

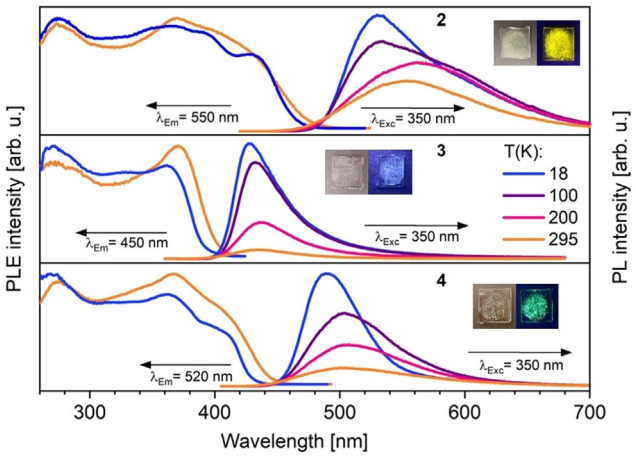

Figure 3. Solid state photoluminescence emission (PL) and excitation (PLE) spectra of tetrametallic complexes **2**, **3**, and **4** (polycrystalline samples) at different temperatures. The PL emission was in each case excited at 350 nm and PLE spectra were recorded at the indicated wavelengths. The photos show samples under daylight and UV lamp illumination.

490 nm (all at 20 K), respectively, show a moderate redshift by increasing the temperature up to 295 K.

A similar energetic order is also observed for the onset of the PLE spectra of **2**–**4** which is well reproduced by our computations (see theoretical section below). The PL quantum yield of polycrystalline samples of **2**–**4** at ambient temperature was determined using an integrating sphere as 55%, 7%, and 32%, respectively. Accordingly, the PL efficiency of **2**–**4** below 100 K approaches 100% for **2** and **4** and 70% for **3**, as estimated from the temperature-dependent emission spectra (Figure 3). The emission of **2**–**4** is phosphorescence, decaying within tens of microseconds (Figure S3.3-1). The effective decay times, τ_{eff}, (derived from biexponential fits) only moderately decrease by increasing the temperature from 20 K to 295 K, well correlating with the decrease of PL intensity. For instance, τ_{eff} of **2** diminishes from 29 μs to 15 μs, accompanied by an approximately twofold decrease of the emission (see above). Despite the efficient PL in the solid state, only a very weak emission was observed for **2** and **4** dissolved in MeCN (Figures S3.2-1, S3.2-3) and practically no emission was detected for **3** in MeCN—presumably due to solvation-aided non-radiative quenching. However, the latter process is apparently inhibited in a rigid surrounding: in frozen MeCN solutions below ca. 200 K complexes **2** and **4** display similarly bright phosphorescence as in the crystalline solid state (Figures S3.4-1, S3.4-3), with the similar spectral position, effective PL lifetime and temperature dependence (Figures S3.4-2, S3.4-4). For instance, the emission maxima in the frozen solutions are observed at 530 nm (**2**) and 485 nm (**4**) below 50 K, which is very close to the values for the crystalline samples. This observation suggests a relatively minor effect of intermolecular interactions in the crystalline complexes on their PL properties. The PLE spectra in solution (both fluid or frozen) correspond to those in the solid state, taking into account that the latter overestimate weak absorption bands due to optically thick sample preparations (and non-validity of the Beer–Lambert law).

In addition to the condensed phase, PL properties of **2** and **4** were studied in gas phase as $[dpfam_2Au_2M_2]^{2+}$ using the trapped ion laser induced fluorescence (TLIF) experiment.[18] In the TLIF setup, ions are brought into gas phase using a nanoelectrospray, mass selected to a single species by a quadrupole mass filter and stored in a liquid-nitrogen-cooled quadrupole ion trap ($T = 83$ K). The ion cloud consisting of up to 10^6 ions was irradiated by a continuous wave laser and luminescence was collected orthogonal to the irradiation direction and detected either by a CCD camera coupled to a spectrograph or by a photon counter for lifetime measurements. Further details on the TLIF setup are given in the Supporting Information.

The relatively strong signals in the TLIF experiment indicate a high PL quantum yield of **2** and **4** also in gas phase, similar to that in the solid state at low temperatures (see above). Figure 4 compares the emission spectra of **2** in the solid state, acetonitrile solution and, as $[dpfam_2Au_2Cu_2]^{2+}$, in gas phase.

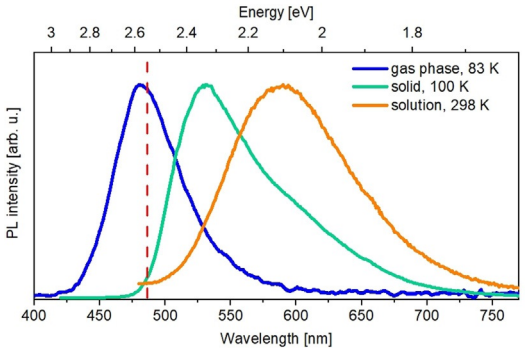

Figure 4. Photoluminescence emission spectra of **2** in solid state, acetonitrile solution, and gas phase (as $[dpfam_2Au_2Cu_2]^{2+}$). The excitation wavelength was 350 nm, 329 nm and 364 nm, respectively. The vertical dashed line indicates the computed $S_0 \leftarrow T_1$ transition.

The emission spectra of **2** show a significant bathochromic shift from the free ions in gas phase (480 nm) to solid state (530 nm) and solution (590 nm), covering, in fact, a large part of the visible spectral range (Figure 4). The shift is expected and typically caused by different stabilization of the ground and emissive states by the environment.[19] On the other hand, only a moderate bathochromic shift of less than 15 nm (< 0.1 eV) was observed for the emission of **4** from gas phase (480 nm at 83 K) to solid state and solution (Figure 5). In the Supporting Information the emissions of **2** and **4** in gas phase are plotted together (Figure S3.1–3). Their maxima in gas phase are only 9 nm or 0.05 eV apart. The PL of **2** and **4** in gas phase is completely quenched by addition of 1% O_2 to the helium buffer gas, indicating that a triplet state is involved in the emission process.

The lifetime of complex **2** was determined to 158 μs (Figure S3.1-2). This is significantly longer than in solid state and solution (ca. 29 μs and 2 μs, respectively, see Figures S3.2-2 and S3.2-4). Again, this behavior is expected, because

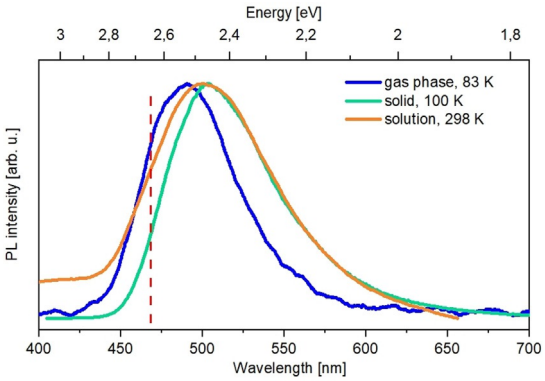

Figure 5. Photoluminescence emission spectra of **4** in solid state, acetonitrile solution, and gas phase (as $[dpfam_2Au_4]^{2+}$). The excitation wavelength was 350, 340, and 364 nm, respectively. The vertical dashed line indicates the computed $S_0 \leftarrow T_1$ transition.

phosphorescence strongly depends on the environment and tends to decay much slower in gas phase.[18] The gas phase lifetime for **4** (68 μs) is significantly shorter than the one for **2**. Finally, gas phase PL of **3** was not detected due to fast dissociation after photoexcitation.

Theoretical Investigations

To assess the nature of the electronic transitions in the tetrametallic complexes **2**–**4**, quantum mechanical calculations using density functional theory with the PBE0[20] functional and a mixed basis set comprising the dhf-TZVPP basis set for Cu, Ag, and Au, and the dhf-SVP basis set for all remaining atoms, were performed.[21] Computational savings were achieved using the RI-*J* approximation in all steps.[22] Excited state energies and geometries were obtained using TDDFT,[23] employing the seminumerical exchange (SENEX)[24] scheme. All calculations were performed using the TURBOMOLE program suite.[25] Further computational details are given in the Supporting Information. Only the dications of **2**–**4** were considered. Therefore, the results can be directly compared with the PL measurements in gas phase available for **2** and **4**. As the optimized structures exhibit a structure close to an ideal C_{2h} symmetry, we also considered point group symmetry for excited state optimizations, to provide further insight regarding the luminescence properties of these three systems. Figure 6 shows the simulated absorption spectra obtained by superimposing Gaussian functions at the lowest 100 singlet excitation energies with a fwhm of 0.3 eV. Note that since the TLIF setup operates with only a few discrete UV laser excitation wavelengths, gas phase PLE spectra are not available for comparison with the computed ordinary absorption spectra. Still, the latter may be compared with experimental measurements in solid state to give a rough estimate of the character of the underlying transitions. Non-relaxed difference densities are obtained following an analogous procedure as described in Ref. [26] and comprise all excitations in a given energetic interval, weighted by their respective oscillator strength. Regions of

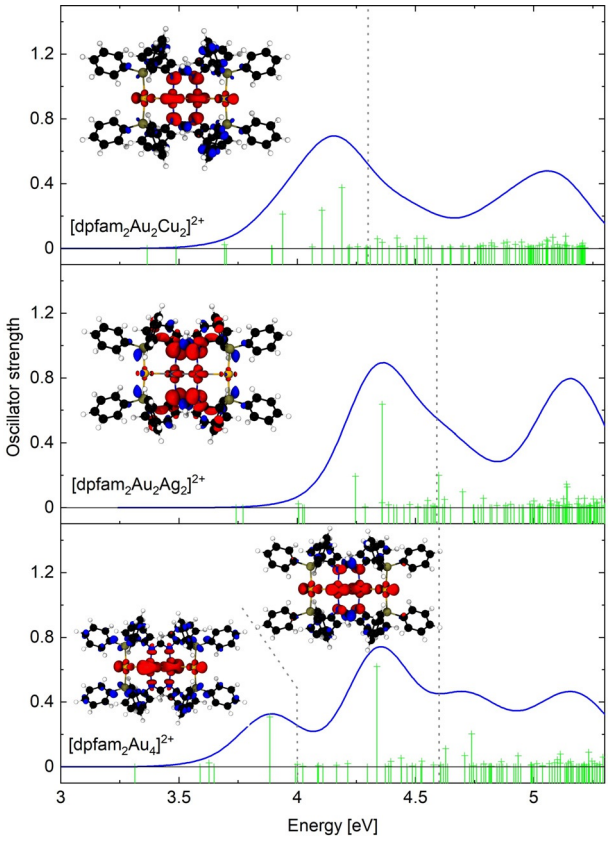

Figure 6. Calculated singlet excitation energies of $[dpfam_2Au_2Cu_2]^{2+}$ (top), $[dpfam_2Au_2Ag_2]^{2+}$ (middle), and $[dpfam_2Au_4]^{2+}$ (bottom) with corresponding oscillator strengths (green). Simulated spectra are obtained by superimposing Gaussians with a fwhm of 0.3 eV at each transition (blue). The character of selected features is depicted using non-relaxed difference densities, including transitions in an energetic range indicated by dashed lines. An electron density loss (gain) is indicated by red (blue).

electron density loss are shown as red contours, while an electron density gain is indicated as blue contours. The bands appear to relate mainly to a density loss in the 3d, 4d, or 5d orbitals (for Cu, Ag, and Au, respectively) of the central two metal atoms, with contributions from 5d orbitals of the outer Au atoms as part of the ligand system. For the major bands a transfer of density to the π* system of the RN^NR bridging fragment and the π* orbitals of the neighboring phenyl groups is observed. This picture is complemented by a Mulliken population analysis given in the Supporting Information (Table S4.9-1). For comparison with the PL emission spectra, the energies of the lowest $S_0 \leftarrow T_1$ (and $S_0 \leftarrow S_1$) transitions of dications of **2**–**4** were calculated in the respective excited state geometry starting from either the C_1 or the C_{2h} symmetric systems. In the latter case all irreducible representations were considered, but only the lowest-lying one is discussed in the following. The excitation energies are presented in Table 1 together with the available experimentally observed emission maxima in different phases. We find a good agreement between experimentally observed luminescence energies at 2.54 eV and calculated triplet excitation energies in excited state geometries at 2.65 eV in the A (C_1) and A_g (C_{2h})

Table 1: Experimental emission maxima and calculated transition energies (in eV) for the tetrametallic complexes **2**–**4**. Additionally, the lowest-lying triplet excitations obtained using symmetry constraints are listed. Irreducible representations are given in parenthesis.

	Exp.			PBE0[a]			
Geometry	Solid state	Solution	Gas phase[b]	$S_0 \rightarrow S_1$ S_0 (C_1)	$S_0 \leftarrow S_1$ S_1 (C_1)	$S_0 \leftarrow T_1$ T_1 (C_1)	$S_0 \leftarrow T_1$ T_1 (C_{2h})
$[dpfam_2Au_2Cu_2]^{2+}$	2.34 (20 K)	2.10 (295 K)	2.58 (83 K)	3.36	3.14	2.55	2.83 (A_g)
$[dpfam_2Au_2Ag_2]^{2+}$	2.90 (18 K)	n/a	n/a	3.74	2.90	2.51[c]	2.97 (B_g)[d]
$[dpfam_2Au_4]^{2+}$	2.53 (20 K)	2.46 (295 K)	2.54 (83 K)	3.31	2.86	2.65	2.65 (A_g)

[a] Computed and [b] measured for dications of **2**–**4**. TDDFT calculations employed the PBE0 functional. S_0, S_1, and T_1 indicate the optimized geometries. [c] Using the TDA the optimized excitation energy was found at 2.82 eV (see Supporting Information). [d] The order of the HOMO and HOMO−1 is reversed for **3**.

irreducible representations for **4**, with an error of approximately 0.1 eV. Note that the symmetry constraints appear to have no significant impact on the transition energy nor character, as in both cases transitions mainly feature contributions from the HOMO and LUMO. For $[dpfam_2Au_2Cu_2]^{2+}$, the lowest-lying triplet excitation in T_1 geometry is found at 2.83 eV in A_g using symmetry constraints. This is significantly higher than the experimentally observed 2.58 eV in gas phase. By relaxing the constraints, we observe an asymmetric distortion of the Au−Cu bonds, from 270 pm to 258 pm and 285 pm, when compared to results in A_g symmetry. The Cu−Cu bond distance is found to be approximately 253 pm in both cases, which is slightly shorter than in the optimized ground state at 260 pm. This gives rise to a more local character of the respective triplet transition. The energy is hereby lowered by 0.28 eV from 2.83 to 2.55 eV and practically coincides with the gas phase experiment. Figure 7 depicts the natural transition orbitals (NTOs) for $[dpfam_2Au_2Cu_2]^{2+}$ in both cases.

The character of the underlying transition appears to be of similar nature as in **4**, involving mostly contributions from the HOMO and LUMO. A possible explanation for the absence of this deformation in **4** may lie in the difference in van der Waals radii of the central metal atoms Cu and Au. Unfortunately, no gas phase data could be recorded for **3** which shows a large difference in the $S_0 \leftarrow T_1$ transition between C_1 and C_{2h}, at 2.51 eV and 2.97 eV respectively. While the latter transition (B_g) follows the character of **2** and **4**, using no symmetry constraint a more complicated excitation vector is observed, with significant contributions from HOMO−2 to HOMO and LUMO to LUMO + 4. Furthermore, in contrast to the homologues **2** and **4**, as well as the results for B_g, the dominant NTOs were found to be largely localized to a single phenyl group, with considerably reduced contributions from the central metal atom (see Supporting Information). We note a significant change in character for the first triplet excitation during geometry optimization.

Complementary calculations using the Tamm–Dancoff approximation (TDA) are given in the Supporting Information and show only minor deviations for **2** and **4**, while the respective $S_0 \leftarrow T_1$ excitation energy for **3** is found at 2.82 eV significantly higher than the value found by TDDFT. The optimized triplet geometry also suggests a slight asymmetric distortion as in $[dpfam_2Au_2Cu_2]^{2+}$ (Table S4.10-1). This may be due to the degree of spin-contamination present in the initial result for **3**. As no gas phase luminescence could be observed for this system, the nature of this transition remains unclear and the results for **3** should be treated with caution. Dielectric screening effects on the triplet excitation energies due to the MeCN solvent were assessed using the conductor-like screening model (COSMO)[27] and imply only a minor effect for **2** and **4**, a brief discussion of which is given in the Supporting Information.

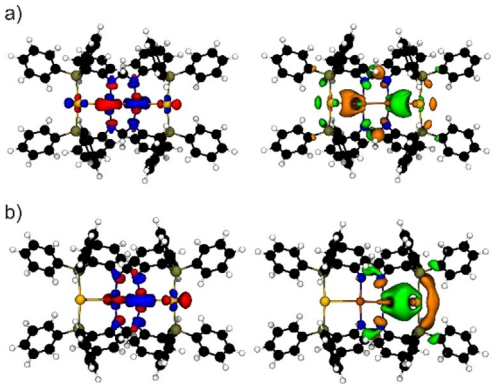

Figure 7. Hole (left) and particle (right) natural transition orbitals (NTOs) of $[dpfam_2Au_2Cu_2]^{2+}$ in the optimized triplet (T1) geometry assuming a C_{2h} symmetric motif (a), in which case the lowest triplet excitation transforms as A_g, or without symmetry constraints (b). The isovalue was set to 0.04 $a_0^{-3/2}$. The respective weights of the depicted NTOs are 92% (a) and 97% (b).

Conclusion

A series of tetrametallic coinage metal complexes was obtained via a straightforward synthetic building block protocol, using digold compound **1** as metalloligand. Its vacant amidinate pocket was subsequently occupied to yield tetrametallic complexes comprising an Au-M-M-Au (M = Cu (**2**), Ag (**3**), Au (**4**)) metal chain with metallophilic interactions. These compounds show bright phosphorescence in the crystalline solid state, also at ambient temperature, with high quantum yields of 55% for **2** and 32% for **4**. Furthermore, efficient phosphorescence was also measured for frozen MeCN solutions of **2** and **4**, as well as for dications of **2** and **4** in gas phase. In contrast, the PL of **2**–**4** in fluid solution (MeCN) is very weak. According to TDDFT calculations, the electronic properties of the Au-M-M-Au complexes can be strongly modulated by metallophilic Au−M interactions. The calculated emission energies of ionic **4** and particularly **2** are

in remarkable agreement with the experimental values. Our results demonstrate that gas phase PL spectroscopy combined with quantum chemical calculations can provide an important reference point for understanding the effects of molecular environment on the electronic/PL properties of metallo-organic compounds.

Acknowledgements

We thank Dr. T. Simler for his help with the interpretation of the NMR spectra and H. Berberich for the various NMR measurements. We thank Dr. T. P. Seifert for fruitful discussions. Financial support by the DFG-funded transregional collaborative research center SFB/TRR 88 "Cooperative Effects in Homo and Heterometallic Complexes (3MET)" is gratefully acknowledged (projects C1, C3, and C7). M.D. thanks the "Fonds der Chemischen Industrie" for the generous fellowship (No. 103581). Open Access funding enabled and organized by Projekt DEAL.

Conflict of Interest

The authors declare no conflict of interest.

Keywords: coinage metals · metallophilicity · phase-dependent photoluminescence · TDDFT

[1] a) S. Schäfer, M. T. Gamer, S. Lebedkin, F. Weigend, M. M. Kappes, P. W. Roesky, *Chem. Eur. J.* **2017**, *23*, 12198; b) M. T. Dau, J. R. Shakirova, A. J. Karttunen, E. V. Grachova, S. P. Tunik, A. S. Melnikov, T. A. Pakkanen, I. O. Koshevoy, *Inorg. Chem.* **2014**, *53*, 4705.

[2] a) T. P. Seifert, S. Bestgen, T. J. Feuerstein, S. Lebedkin, F. Krämer, C. Fengler, M. T. Gamer, M. M. Kappes, P. W. Roesky, *Dalton Trans.* **2019**, *48*, 15427; b) M.-M. Zhang, X.-Y. Dong, Z.-Y. Wang, H.-Y. Li, S.-J. Li, X. Zhao, S.-Q. Zang, *Angew. Chem. Int. Ed.* **2020**, *59*, 10052; *Angew. Chem.* **2020**, *132*, 10138; c) P. Alam, C. Climent, P. Alemany, I. R. Laskar, *J. Photochem. Photobiol. C* **2019**, *41*, 100317; d) T. P. Seifert, V. R. Naina, T. J. Feuerstein, N. D. Knöfel, P. W. Roesky, *Nanoscale* **2020**, *12*, 20065; e) R. L. White-Morris, M. M. Olmstead, F. Jiang, D. S. Tinti, A. L. Balch, *J. Am. Chem. Soc.* **2002**, *124*, 2327; f) M. Saitoh, A. L. Balch, J. Yuasa, T. Kawai, *Inorg. Chem.* **2010**, *49*, 7129; g) R. L. White-Morris, M. M. Olmstead, S. Attar, A. L. Balch, *Inorg. Chem.* **2005**, *44*, 5021; h) A. L. Balch, *Angew. Chem. Int. Ed.* **2009**, *48*, 2641; *Angew. Chem.* **2009**, *121*, 2679; i) D. Rios, D. M. Pham, J. C. Fettinger, M. M. Olmstead, A. L. Balch, *Inorg. Chem.* **2008**, *47*, 3442.

[3] a) N. L. Coker, J. A. Krause Bauer, R. C. Elder, *J. Am. Chem. Soc.* **2004**, *126*, 12; b) Q.-M. Wang, Y.-A. Lee, O. Crespo, J. Deaton, C. Tang, H. J. Gysling, M. Concepción Gimeno, C. Larraz, M. D. Villacampa, A. Laguna, R. Eisenberg, *J. Am. Chem. Soc.* **2004**, *126*, 9488; c) J. R. Shakirova, E. V. Grachova, V. V. Gurzhiy, I. O. Koshevoy, A. S. Melnikov, O. V. Sizova, S. P. Tunik, A. Laguna, *Dalton Trans.* **2012**, *41*, 2941.

[4] a) N. Tsukada, O. Tamura, Y. Inoue, *Organometallics* **2002**, *21*, 2521; b) L. Wesemann, H. Schubert, H. Mayer, S. Wernitz (Eberhard Karls Universität Tübingen), DE 10 2011 079 857 A1, **2011**; c) K.-s. Son, D. M. Pearson, S.-J. Jeon, R. M. Waymouth, *Eur. J. Inorg. Chem.* **2011**, 4256; d) S. Tanaka, A. Yagyu, M. Kikugawa, M. Ohashi, T. Yamagata, K. Mashima, *Chemistry* **2011**, *17*, 3693 – 3709; e) Y. Yamaguchi, K. Yamanishi, M. Kondo, N. Tsukada, *Organometallics* **2013**, *32*, 4837 – 4842; f) M. Dahlen, N. Reinfandt, C. Jin, M. T. Gamer, K. Fink, P. W. Roesky, *Chem. Eur. J.* **2021**, https://doi.org/10.1002/chem.202102430.

[5] H. Schmidbaur, A. Schier, *Chem. Soc. Rev.* **2012**, *41*, 370.

[6] a) P. Pyykkö, J. Li, N. Runeberg, *Chem. Phys. Lett.* **1994**, *218*, 133; b) E. Andris, P. C. Andrikopoulos, J. Schulz, J. Turek, A. Růžička, J. Roithová, L. Rulíšek, *J. Am. Chem. Soc.* **2018**, *140*, 2316; c) P. K. Mehrotra, R. Hoffmann, *Inorg. Chem.* **1978**, *17*, 2187; d) A. Dedieu, R. Hoffmann, *J. Am. Chem. Soc.* **1978**, *100*, 2074; e) Y. Jiang, S. Alvarez, R. Hoffmann, *Inorg. Chem.* **1985**, *24*, 749 ; f) M. Jansen, *J. Less. Common. Met.* **1980**, *76*, 285.

[7] a) F. Scherbaum, A. Grohmann, G. Müller, H. Schmidbaur, *Angew. Chem. Int. Ed. Engl.* **1989**, *28*, 463; *Angew. Chem.* **1989**, *101*, 464; b) H. Schmidbaur, A. Schier, *Chem. Soc. Rev.* **2008**, *37*, 1931; c) V. G. Andrianov, Y. T. Struchkov, E. R. Rossinskaja, *J. Chem. Soc. Chem. Commun.* **1973**, 338; d) P. G. Jones, *Gold Bull.* **1981**, *14*, 102; e) M. Melnínk, R. V. Parish, *Coord. Chem. Rev.* **1986**, *70*, 157.

[8] a) X.-Y. Chang, G.-T. Xu, B. Cao, J.-Y. Wang, J.-S. Huang, C.-M. Che, *Chem. Sci.* **2017**, *8*, 7815; b) V. W.-W. Yam, K. M.-C. Wong, *Chem. Commun.* **2011**, *47*, 11579; c) V. W.-W. Yam, V. K.-M. Au, S. Y.-L. Leung, *Chem. Rev.* **2015**, *115*, 7589; d) T. A. C. A. Bayrakdar, T. Scattolin, X. Ma, S. P. Nolan, *Chem. Soc. Rev.* **2020**, *49*, 9099; e) M. Bardajía, A. Laguna, *Eur. J. Inorg. Chem.* **2003**, 3069; f) M. J. Calhorda, C. Ceamanos, O. Crespo, M. C. Gimeno, A. Laguna, C. Larraz, P. D. Vaz, M. D. Villacampa, *Inorg. Chem.* **2010**, *49*, 8255; g) A. Burini, J. P. Fackler, R. Galassi, T. A. Grant, M. A. Omary, M. A. Rawashdeh-Omary, B. R. Pietroni, R. J. Staples, *J. Am. Chem. Soc.* **2000**, *122*, 11264; h) P. Ai, A. A. Danopoulos, P. Braunstein, K. Y. Monakhov, *Chem. Commun.* **2014**, *50*, 103; i) A. P. Marchenko, H. N. Koidan, A. N. Hurieva, O. V. Gutov, A. N. Kostyuk, C. Tubaro, S. Lollo, A. Lanza, F. Nestola, A. Biffis, *Organometallics* **2013**, *32*, 718; j) S. Raju, H. B. Singh, R. J. Butcher, *Dalton Trans.* **2020**, *49*, 9099 – 9117; k) M. Jansen, *Angew. Chem. Int. Ed. Engl.* **1987**, *26*, 1098; *Angew. Chem.* **1987**, *99*, 1136.

[9] a) M. B. Brands, J. Nitsch, C. F. Guerra, *Inorg. Chem.* **2018**, *57*, 2603; b) V. W.-W. Yam, E. Chung-Chin Cheng in *Photochemistry and photophysics of coordination compounds II*, *Vol. 281* (Eds.: V. Balzani, S. Campagna, A. Barbieri), Springer, Berlin, **2007**, pp. 269; c) J. Li, P. Pyykkö, *Chem. Phys. Lett.* **1992**, *197*, 586; d) Q. Zheng, S. Borsley, G. S. Nichol, F. Duarte, S. L. Cockroft, *Angew. Chem. Int. Ed.* **2019**, *58*, 12617; *Angew. Chem.* **2019**, *131*, 12747.

[10] a) R. L. White-Morris, M. M. Olmstead, A. L. Balch, *J. Am. Chem. Soc.* **2003**, *125*, 1033; b) H. Schmidbaur, A. Schier, *Angew. Chem. Int. Ed.* **2015**, *54*, 746; *Angew. Chem.* **2015**, *127*, 756.

[11] a) I. O. Koshevoy, Y.-C. Chang, A. J. Karttunen, M. Haukka, T. Pakkanen, P.-T. Chou, *J. Am. Chem. Soc.* **2012**, *134*, 6564; b) M. A. Malwitz, S. H. Lim, R. L. White-Morris, D. M. Pham, M. M. Olmstead, A. L. Balch, *J. Am. Chem. Soc.* **2012**, *134*, 10885.

[12] M. Dahlen, M. Kehry, S. Lebedkin, M. M. Kappes, W. Klopper, P. W. Roesky, *Dalton Trans.* **2021**, https://doi.org/10.1039/d1dt02226a.

[13] a) M. Stollenz, *Chem. Eur. J.* **2019**, *25*, 4274; b) H. de la Riva, M. Nieuwhuyzen, C. Mendicute Fierro, P. R. Raithby, L. Male, M. C. Lagunas, *Inorg. Chem.* **2006**, *45*, 1418.

[14] P. N. Bartlett, F. Cheng, D. A. Cook, A. L. Hector, W. Levason, G. Reid, W. Zhang, *Inorg. Chim. Acta* **2010**, *363*, 1048.

[15] M. Gil-Moles, M. C. Gimeno, J. M. López-de-Luzuriaga, M. Monge, M. E. Olmos, D. Pascual, *Inorg. Chem.* **2017**, *56*, 9281.

[16] a) Y. Takemura, H. Takenaka, T. Nakajima, T. Tanase, *Angew. Chem. Int. Ed.* **2009**, *48*, 2157; *Angew. Chem.* **2009**, *121*, 2191.

[17] a) T. Tanase, R. Otaki, T. Nishida, H. Takenaka, Y. Takemura, B. Kure, T. Nakajima, Y. Kitagawa, T. Tsubomura, *Chem. Eur. J.* **2014**, *20*, 1577; b) D. Li, C.-M. Che, S.-M. Peng, S.-T. Liu, Z.-Y. Zhou, T. C. W. Mak, *J. Chem. Soc. Dalton Trans.* **1993**, 189.
[18] M. Kordel, D. Schooss, C. Neiss, L. Walter, M. M. Kappes, *J. Phys. Chem. A* **2010**, *114*, 5509.
[19] J. R. Lakowicz, *Principles of Fluorescence Spectroscopy*, *Vol. 1*, Springer, Cham, **2006**.
[20] C. Adamo, V. Barone, *J. Chem. Phys.* **1999**, *110*, 6158.
[21] a) M. Kühn, F. Weigend, *J. Chem. Theory Comput.* **2013**, *9*, 5341; b) F. Weigend, R. Ahlrichs, *Phys. Chem. Chem. Phys.* **2005**, *7*, 3297; c) F. Weigend, A. Baldes, *J. Chem. Phys.* **2010**, *133*, 174102; d) D. Figgen, G. Rauhut, M. Dolg, H. Stoll, *Chem. Phys.* **2005**, *311*, 227.
[22] K. Eichkorn, F. Weigend, O. Treutler, R. Ahlrichs, *Theor. Chim. Acta* **1997**, *97*, 119.
[23] a) R. Bauernschmitt, M. Häser, O. Treutler, R. Ahlrichs, *Chem. Phys. Lett.* **1997**, *264*, 573; b) R. Bauernschmitt, R. Ahlrichs, *Chem. Phys. Lett.* **1996**, *256*, 454; c) R. Bauernschmitt, R. Ahlrichs, *J. Chem. Phys.* **1996**, *104*, 9047; d) F. Furche, R. Ahlrichs, *J. Chem. Phys.* **2002**, *117*, 7433; e) D. Rappoport, F. Furche, *J. Chem. Phys.* **2005**, *122*, 064105.
[24] a) C. Holzer, *J. Chem. Phys.* **2020**, *153*, 184115; b) F. Neese, F. Wennmohs, A. Hansen, U. Becker, *Chem. Phys.* **2009**, *356*, 98; c) P. Plessow, F. Weigend, *J. Comput. Chem.* **2012**, *33*, 810.
[25] a) R. Ahlrichs, M. Bär, M. Häser, H. Horn, C. Kolmel, *Chem. Phys. Lett.* **1989**, *162*, 165; b) F. Furche, R. Ahlrichs, C. Hättig, W. Klopper, M. Sierka, F. Weigend, *Wiley Interdiscip. Rev.: Comput. Mol. Sci.* **2014**, *4*, 91.
[26] M. Kühn, F. Weigend, *J. Chem. Phys.* **2014**, *141*, 224302.
[27] A. Klamt, G. Schüürmann, *J. Chem. Soc. Perkin Trans. 2* **1993**, 799.
[28] Deposition Numbers 2041039 (**2**), 2041040 (**3**), and 2041041 (**4**) contain the supplementary crystallographic data for this paper. These data are provided free of charge by the joint Cambridge Crystallographic Data Centre and Fachinformationszentrum Karlsruhe Access Structures service www.ccdc.cam.ac.uk/structures.

Manuscript received: July 27, 2021
Accepted manuscript online: August 20, 2021
Version of record online: September 24, 2021

